Reaction Mechanisms

DOI: 10.1002/anie.201104147

Characterization of the Reaction Path and Transition States for RNA Transphosphorylation Models from Theory and Experiment**

Kin-Yiu Wong, Hong Gu, Shuming Zhang, Joseph A. Piccirilli,* Michael E. Harris,* and Darrin M. York**

The elucidation of the chemical mechanisms whereby biological molecules control, regulate, and catalyze phosphoryl-transfer reactions has profound implications for processes such as transcription, energy storage and transfer, cell signaling, and gene regulation.[1,2] In particular, the catalytic properties of RNA have applications in the design of new biotechnologies, and are also implicated in the evolutionary origins of life itself.[3] The characterization of the transition state for any given reaction is of primary importance in understanding the reaction mechanism. Kinetic isotope effects (KIEs) offer one of the most powerful and sensitive experimental probes with which to investigate the chemical environment of transition states.[4–6] However, theoretical methods are required to assist in the interpretation of experimental measurements of complex reactions, and to produce a detailed mechanistic model that traces the pathway from the reactant state, through the transition state, and into the product state. [7,8]

Herein, we present experimental and computational results that characterize the mechanism of model phosphoryl transfer reactions, that mimic RNA cleavage transesterification that is catalyzed by enzymes, such as RNase A,[1] as well as endonucleolytic ribozymes, such as the hammerhead, hairpin, hepatitis delta virus (HDV), Varkud satellite (VS), and glucosamine-6-phosphate-activated (glmS) ribozymes.[9–11] Secondary KIE values for the cleavage transesterification of a dinucleotide system are also reported. These KIE values, together with primary isotope effect measurements from previous reports,[12,13] represent a comprehensive characterization of isotope effects for a native (unmodified) RNA system.

Scheme 1 illustrates the general mechanism for the reverse, dianionic, in-line methanolysis of ethylene phosphate, which is a model for base-catalyzed RNA phosphate transesterification. The phosphoryl oxygen positions are labeled in accordance with their RNA counterparts. The free energy profiles for Scheme 1 were determined through density-functional quantum mechanical/molecular mechanical (QM/MM) simulations in explicit solvent (Figure 1, top graph).[14–17] These simulations take into account the dynamic fluctuations of the solute and the degrees of freedom of the solvent in determining the free energy profiles. In addition, the adiabatic reaction energy profiles with solvation effects treated implicitly with a polarizable continuum model (PCM)[18] were determined (Figure 1). The PCM model was specifically calibrated for the native model compound, as well as the 3′- and 5′-thio-substituted compounds (referred to hereafter as $S^{3'}$ and $S^{5'}$, respectively; Figure 1). The $S^{3'}$ and $S^{5'}$ compounds are models for the corresponding chemically modified RNAs that serve as valuable experimental probes of phosphoryl transfer mechanisms catalyzed by ribozymes.[19] For example, the $S^{5'}$ substitution in the HDV ribozyme serves as an enhanced leaving group that suppresses the deleterious effect of a mutation of a critical cytosine residue, which has been interpreted to support its role as a general acid catalyst.[20]

The energy values for stationary points of the reactions with the native and thio-substituted compounds are shown in Table 1. By using our recently developed ab initio path-integral method, which is based on Kleinert's variational perturbation theory,[7,21–23] we also calculated the KIE values. These KIE values are shown along with the most relevant experimental values for comparison in Table 2. The agreement between the theoretical and experimental results allows for a detailed mechanistic interpretation based on the theoretical models.[7,8]

All of the profiles calculated in this study correspond to associative (or concerted) mechanisms, characterized by an initial nucleophilic attack, as is typical for phosphate diesters.[6] The departure of the leaving group can occur at the same time as the nucleophilic attack (as in the reaction with the $S^{5'}$ compound) or can occur in a stepwise fashion, which

[*] Dr. K.-Y. Wong, Prof. D. M. York
BioMaPS Institute for Quantitative Biology
Department of Chemistry and Chemical Biology
Rutgers, The State University of New Jersey
610 Taylor Road, Piscataway, NJ 08854 (USA)
E-mail: wongky@biomaps.rutgers.edu
kiniu@alumni.cuhk.net
york@biomaps.rutgers.edu

Dr. H. Gu, Dr. S. Zhang, Prof. M. E. Harris
RNA Center and Department of Biochemistry
Case Western Reserve University School of Medicine
Cleveland, OH 44106 (USA)
E-mail: michael.e.harris@case.edu

Prof. J. A. Piccirilli
Department of Biochemistry and Molecular Biology and
Department of Chemistry, University of Chicago
Chicago, Illinois 60637 (USA)
E-mail: jpicciri@uchicago.edu

[**] We are grateful for financial support from the National Institutes of Health (GM062248 to D.M.Y., R21GM079647 to M.E.H., and AI081987 to J.A.P.). Computational resources were provided by the Minnesota Supercomputing Institute (MSI) and by the NSF TeraGrid through the Texas Advanced Computing Center and National Institute for Computational Sciences, under grant number TG-CHE100072.

Supporting information for this article is available on the WWW under http://dx.doi.org/10.1002/anie.201104147.

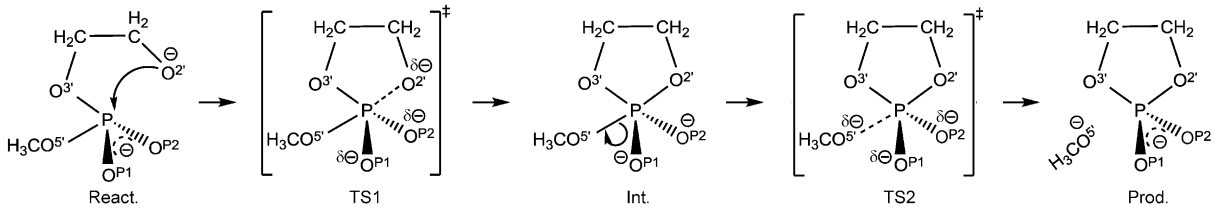

Scheme 1. General reaction scheme for the (associative) reverse of dianionic in-line methanolysis of ethylene phosphate: a model for RNA phosphate transesterification under alkaline conditions. "React", "TS1", "Int.", "TS2", and "Prod." stand for reactant, transiton state 1, intermediate, transition state 2, and product, respectively. In the present work, the native reaction shown in the scheme is studied as well as reactions that incorporate single sulfur substitutions in the bridging 3′- ($S^{3'}$) and leaving group 5′-positions ($S^{5'}$). Note: as revealed by the computational analysis, not all of the states shown in the scheme exist for every reaction (see text for details).

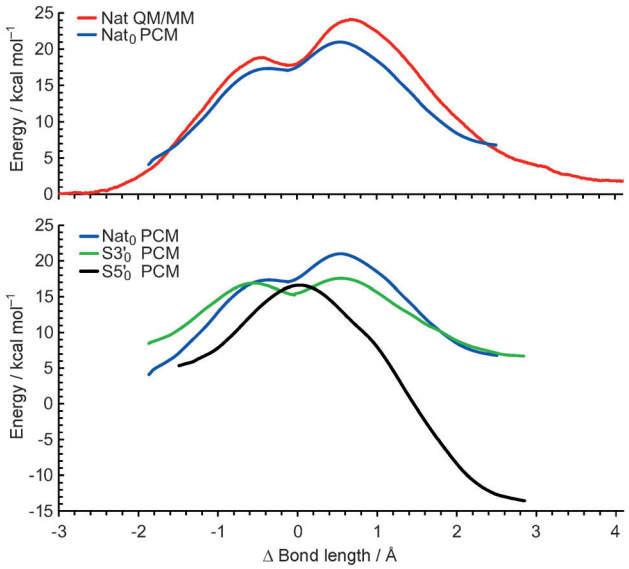

Figure 1. Comparison of density-functional QM/MM free energy and adiabatic PCM profiles for the reaction with the native model compound (top graph), and density-functional adiabatic PCM profiles for the reaction with native, $S^{3'}$, and $S^{5'}$ model compounds (bottom graph) as a function of the difference in bond length (Δbond) between the breaking P–$X^{5'}$ bond (X = O for native and $S^{3'}$; X = S for $S^{5'}$) and the forming P–$O^{2'}$ bond (Δbond = P–$X^{5'}$–P–$O^{2'}$). The adiabatic PCM profiles are mapped from the intrinsic reaction coordinate paths and have been shifted to match the respective rate-controlling free energy barriers calculated in the decoupled, rigid-rotor, harmonic-oscillator approximation[26] at 37 °C. However, aside from this shift, the adiabatic PCM profiles do not otherwise include zero-point energy or thermal corrections to the free energy, unlike the numbers listed in the last three rows of Table 1.

Table 1: Relative free energy (kcal mol^{-1}) and reaction coordinate values (Δbond) calculated for stationary points along the coordinate of the native, $S^{3'}$, and $S^{5'}$ models.[a]

Reaction	TS1		Int.		TS2	
	$\Delta G^{\ddagger}$	Δbond	ΔG	Δbond	$\Delta G^{\ddagger}$	Δbond
Nat QM/MM	18.8[b]	−0.43	17.7[b]	−0.12	**24.1**[b,c]	0.67
Nat_0 PCM	17.3	−0.36	17.0	−0.12	**21.0**[c]	0.54
Nat PCM	18.6	−0.36	18.3	−0.12	**21.0**[c]	0.54
$S^{3'}$ PCM	**16.9**	−0.55	16.0	−0.04	17.8	0.54
$S^{5'}$ PCM	**16.6**	−0.02	n.a.[d]	n.a.[d]	n.a.[d]	n.a.[d]

[a] Δbond is the difference in bond length between the breaking P–$X^{5'}$ bond (X = O for native and $S^{3'}$; X = S for $S^{5'}$) and the forming P–$O^{2'}$ bond (Δbond = P–$X^{5'}$–P–$O^{2'}$). ΔG values are given in kcal mol^{-1}. Δbond values are given in Å. Nat_0 is the PCM energy (Figure 1) shifted by the thermal corrections at TS2. Values in bold indicate the rate-controlling transition state suggested by comparison with experimental KIE measurements. [b] Statistical uncertainties are 1.1, 0.8, and 1.4 kcal mol^{-1} for TS1, Int., and TS2, respectively. [c] The barrier for UpG transphosphorylation estimated from experiments is 19.9 kcal mol^{-1}.[12] [d] Not applicable as Int. and TS2 were not found.

results in the formation of a stable, pentavalent phosphorane intermediate. In the stepwise mechanism, two transition states occur: one in which the nucleophilic attack occurs (TS1), and another in which the leaving group departs (TS2; Scheme 1). The characterization of these transition states as either "early" or "late" depends on the extent of P–$O^{2'}$ bond formation and P–$O^{5'}$ bond cleavage.

The density-functional QM/MM free energy profile[24,25] and the PCM adiabatic reaction profile for the reaction of the native compound are very similar (Figure 1, top). Both profiles show an associative mechanism and have distinct TS1 and TS2 transition states, which are separated by a shallow, metastable intermediate. In both cases, TS2 is rate-controlling. A comparison of the activation free energy values calculated from the QM/MM simulations and from the adiabatic reaction profiles (which include zero-point and thermal corrections; Table 1) indicates that TS1 has very similar activation energy in the two profiles (18.8 kcal mol^{-1} and 18.6 kcal mol^{-1}, respectively). In contrast, TS2 is 3.1 kcal mol^{-1} higher in energy in the QM/MM simulation. The rate-controlling TS2 has considerable "late" character, in which cleavage of the exocyclic P–$O^{5'}$ bond is advanced (Table 1). This result is derived from a combination of ring-strain effects and differential solvation of the cyclic versus acyclic phosphates.[8,29] The calculated density-functional free energy barrier with PCM solvation (21.0 kcal mol^{-1}) is very similar to that estimated from the experimental rate for UpG transphosphorylation (19.9 kcal mol^{-1}), with extrapolation to the infinite pH limit in the rate expression (that is, assuming that the nucleophile is always in the deprotonated form) and assuming the transmission coefficient as unity.[12] This result, along with the consistent values from the PCM reaction profile and from the QM/MM simulations with explicit solvent (Figure 1, top), suggests that the density-functional PCM calculations sufficiently capture the essential features of the solvation effects on the reaction profile to determine the KIE values. The close agreement between the calculated and

Table 2: Primary KIE values on the 2′ nucleophile ($^{18}k_{Nu}$) and the 5′ leaving group ($^{18,34}k_{Lg}$), and secondary KIE values on O^{1P} ($^{18}k_{O1P}$) and O^{2P} ($^{18}k_{O2P}$) in aqueous solution for TS1 and TS2, along with the most relevant available experimental results for comparison.[a]

Reaction	TS1		TS2		Expt	
	$^{18}k_{Nu}$	$^{18,34}k_{Lg}$	$^{18}k_{Nu}$	$^{18,34}k_{Lg}$	$^{18}k_{Nu}$	$^{18,34}k_{Lg}$
native	1.017	1.006	**0.968**	**1.059**	0.981(3)[b]	1.034(4)[b]
$S^{3'}$	**1.043**[c]	**1.008**[c]	0.992[c]	1.049[c]	1.119(6)[d]	1.0118(3)[d]
$S^{5'}$	**1.042**[c]	**1.002**[c]	n.a.[e]	n.a.[e]	1.025(5)[d]	1.0009(1)[d]
Reaction	TS1		TS2		Expt	
	$^{18}k_{O1P}$	$^{18}k_{O2P}$	$^{18}k_{O1P}$	$^{18}k_{O2P}$	$^{18}k_{O1P}$	$^{18}k_{O2P}$
native	1.004	1.004	**1.005**	**1.003**	0.999(1)[f]	0.999(1)[f]
$S^{3'}$	**1.004**[c]	**1.004**[c]	1.002[c]	1.003[c]	n.d.[g]	n.d.[g]
$S^{5'}$	**1.004**[c]	**1.004**[c]	n.a.[e]	n.a.[e]	n.d.[g]	n.d.[g]

[a] Temperatures used in calculations are identical to those used in the experiments that are being compared: 37 °C for reactions with the native compound, and 80 °C for reactions with $S^{3'}$ and $S^{5'}$ compounds. All primary KIE values are calculated using the second order Kleinert's variational perturbation theory with decoupled instantaneous normal coordinate approximation, and the secondary KIE values are calculated using the Bigeleisen equation in the decoupled, rigid-rotor, harmonic-oscillator approximation.[27,28] Values in bold represent the rate-controlling KIE values, as determined by comparison with experimental KIE measurements. Experimental errors in the last decimal place are given in parenthesis. [b] Extracted from Ref. [12], in which the measured $^{18}k_{Nu}$ value has been corrected for deprotonation. [c] To be consistent with the experiments in Ref. [13], the KIE values are calculated with the nucleophile $O^{2'}$ protonated in the reactant state. [d] Extracted from Ref. [13], in which the nucleophile $O^{2'}$ is protonated in the reactant state. [e] Not applicable as TS2 was not found. [f] Values represent an average observed for O^{1P}- and O^{2P}-positions. [g] Not determined.

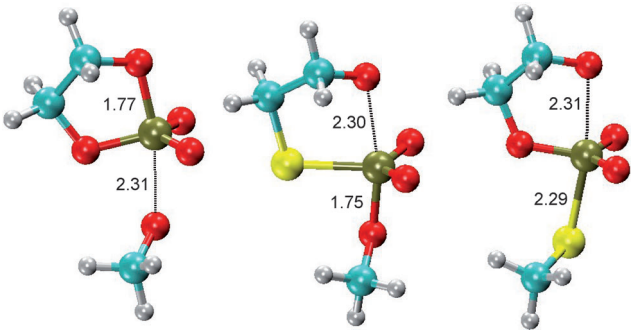

Figure 2. Rate-controlling transition-state structures consistent with experimental KIE values. Left = native; middle = $S^{3'}$; right = $S^{5'}$. The bond lengths are given in Å.

experimental KIE values (Table 2) further supports this supposition.

The primary KIE values which were calculated by using our ab initio path-integral method[7,21–23] are listed in Table 2. These values are in good agreement with the experimental results. The term "good agreement" refers to agreement within the resolution of the KIE values as being large inverse (less than 0.97), inverse (0.97–0.99), near unity (0.99–1.01), normal (1.01–1.03), and large normal (greater than 1.03). In the experiment, the model reaction for RNA transesterification is the base-catalyzed 2′-*O*-transphosphorylation of the RNA dinucleotide 5′-UpG-3′.[12] Since both deprotonation of the 2′-OH group and formation of the P–$O^{2'}$ bond will contribute to the KIE values measured in the experiments, the values reported here for $^{18}k_{Nu}$ and $^{18}k_{Lg}$ (at the infinite pH limit) do not include the equilibrium isotope effect on alcohol deprotonation. The inverse KIE value of $^{18}k_{Nu}$ (0.981) and the large normal KIE value of $^{18}k_{Lg}$ (1.034) measured experimentally[12] for TS2 agree well with the KIE values calculated for TS2 (0.968 and 1.059; Table 2). In contrast to the rate-controlling TS2, the KIE value calculated for $^{18}k_{Nu}$ based on TS1 is normal (1.017), and the KIE value calculated for $^{18}k_{Lg}$ is close to unity (1.006). This finding supports the interpretation that the KIE values measured for the reaction with the native compound (UpG transphosphorylation) are consistent with a rate-controlling transition state that is characterized by an almost fully formed P–$O^{2'}$ bond and an almost fully cleaved P–$O^{5'}$ bond (Table 1 and Figure 2).

The anharmonic contributions to all the calculations of the primary KIE values which were estimated by using our ab initio path-integral method are small (although anharmonicity calculated with our method has been shown to be large for some other reactions[7]). The largest anharmonic contribution is only about 0.3%. Hence, we only calculated the anharmonic contributions in the KIE values for the primary isotopomers (i.e., the atoms of the 2′ nucleophile and 5′ leaving group) listed in Table 2.

In the reaction with the $S^{3'}$ compound, the KIE values measured experimentally correspond to an early transition state. Relative to the reaction with the native compound, the sulfur atom at the 3′-position leads to a reaction profile that is characterized by two transition states, which are separated by a kinetically distinct intermediate (Figure 1, bottom graph and Table 1). The calculated barriers for the two transition states are quite similar to one another (less than 1 kcal mol^{-1} difference). Both barriers are lower than the rate-controlling transition state of the reaction with the native compound by 3 kcal mol^{-1} or more. This result indicates that the rate of reaction for the $S^{3'}$ compound should be faster than the rate of reaction for the native compound. These calculations are consistent with experimental measurements for 3' thio-substituted dinucleotides.[13,30,31] The lower barrier arises from a combination of the stabilizing electronic effects of the soft sulfur atom in the equatorial position of the pentavalent transition state that is able to help delocalize charge, and a partial alleviation of ring strain through the longer P–$S^{3'}$ bond. Solvation effects are also present, but are less pronounced than at the nonbridging positions which carry a formal negative charge.

Despite their similar barrier heights, TS1 and TS2 for the reaction with the $S^{3'}$ compound produced significantly different primary KIE signatures. The primary KIE values calculated for TS1 are large normal and close to unity for the nucleophile ($^{18}k_{Nu}$) and leaving group ($^{18}k_{Lg}$), respectively. In contrast, the primary KIE values calculated for TS2 are near unity and large normal for the nucleophile ($^{18}k_{Nu}$) and leaving group ($^{18}k_{Lg}$), respectively (Table 2). The experimental KIE values for the reaction with a *m*-nitrobenzyl leaving group ($pK_a = 14.9$) are anomalously large normal ($^{18}k_{Nu} = 1.119$)[32–34] and moderate normal ($^{18}k_{Lg} = 1.012$) for nucleophile and leaving group,[13] respectively. This is consistent with

the signature of the TS1 transition state (Table 2 and Figure 2). This experimental $^{18}k_{Nu}$ value[13] reflects a reaction from the ground state in which the 2′-oxygen atom is not deprotonated, and includes a somewhat large normal contribution of 2–4% from the equilibrium isotope effect on alcohol deprotonation. Accordingly, the KIE values were calculated including this contribution. As in the case for the reaction with the native compound, the secondary KIE values that were calculated for the O^{1P} and the O^{2P} atoms for the reaction with the $S^{3'}$ compound are close to unity (Table 2).

The sulfur substitution at the 5′-position results in a reaction profile that is unimodal, and the activation energy is lower than in the reaction profiles of the native and $S^{3'}$ compounds (Figure 1, bottom, and Table 1). Although sulfur is less apicophilic than oxygen in pentavalent phosphorus compounds,[35] this effect is not predicted to be large in the present calculations, because the free energy of formation of TS1 in the reaction with the $S^{5'}$ compound is only 2 kcal mol^{-1} lower than for the reaction with the native compound. The main contribution to the differences in the reaction profiles of the native and $S^{5'}$ compounds is derived from the thiolate being an enhanced leaving group, relative to the methoxide anion (the pK_a value of primary alcohols is typically around 5 pK_a units higher than the corresponding thiols). The difference in leaving group leads to the elimination of TS2 from the profile of the reaction, and a shift towards an early transition state character (a smaller P–$O^{2'}$ bond order). The value of Δbond in Table 1 and Figure 2 for the transition state is −0.02 Å, but this value reflects the fact that the bond length of P–$S^{5'}$ is approximately 0.5 Å longer than the P–$O^{5'}$ bond. The rate-controlling barrier for the reaction with the $S^{5'}$ compound is approximately 16.6 kcal mol^{-1}, which is the smallest of the reaction models studied here. The size of this barrier suggests that this substitution reaction will have the fastest rate. This result is consistent with experimental studies of 5′-substituted reaction models.[13,36,37]

The primary KIE values predicted for both $^{18}k_{Nu}$ (1.042) and $^{34}k_{Lg}$ (1.002) for the reaction with the $S^{5'}$ compound (Table 2) are large normal and close to unity, respectively, and are in agreement with the experimental results ($^{18}k_{Nu}$: 1.025; $^{34}k_{Lg}$: 1.001) for the cyclization of *m*-nitrobenzyl ribonucleoside phosphodiester with $S^{5'}$ substitution.[13] This agreement supports the notion that the rate-controlling transition state for the reaction with the $S^{5'}$ compound is TS1.

The secondary KIE values for the nonbridging phosphoryl oxygen positions in the reaction with the native UpG dinucleotide were measured (Table 2). The present model system involves an associative reaction with a dianionic phosphate diester and the added complexity of coupling between the vibrational modes of the ring in the formation of the transition state. The KIE values which were measured for the nonbridging phosphoryl oxygen positions were very close to unity (0.999). Within the error ranges, these KIE values are in good agreement with the KIE values of 1.003–1.005 which were calculated for the reaction with the native compound (Table 2). Unlike the calculated differences between the primary KIE values, the secondary KIE values for the reactions with the native, $S^{3'}$, and $S^{5'}$ compounds, were all close to unity.

In conclusion, we have reported the density-functional combined QM/MM simulations and solvated adiabatic reaction profiles for model transphosphorylation reactions of native and thio-substituted RNA. The KIE values were calculated by using our recently developed ab initio path-integral method,[7,21–23] which takes into account the treatment of internuclear quantum effects. Additionally, we measured the secondary KIE values for the reaction of native UpG. This dinucleotide sequence represents the cleavage site in the HDV ribozyme,[9,12] and we predicted the secondary KIE values for reactions with thio-substituted analogues. Our results provide an atomic-level picture of the reactions, which includes a detailed characterization of the rate-controlling transition states. These transition states are in agreement with experimental measurements of the rates of reaction and the primary and secondary KIE values. The reaction with the native compound is characterized by a rate-controlling transition state which corresponds to exocyclic bond cleavage of the leaving group. This reaction also has an inverse primary nucleophile KIE value. The reaction with the $S^{3'}$ compound is characterized by two distinct transition states. The transition state which corresponds to the nucleophilic attack, rather than the departure of the leaving group, gives rise to the large normal primary nucleophile KIE value which was observed in experiments. The reaction with the $S^{5'}$ compound is concerted, has a unimodal reaction profile with the lowest barrier, and has large normal primary KIE values. Unlike the striking differences between the primary KIE values which were calculated for the reactions with the native and thio-substituted compounds, all of the secondary KIE values are close to unity. Together, these results paint a detailed picture of the reaction mechanisms of model phosphoryl-transfer reactions.

Received: June 16, 2011
Revised: October 6, 2011
Published online: November 11, 2011

Keywords: ab initio calculations · kinetic isotope effects · reaction mechanisms · RNA · transphosphorylation

[1] D. M. Perreault, E. V. Anslyn, *Angew. Chem.* **1997**, *109*, 470; *Angew. Chem. Int. Ed. Engl.* **1997**, *36*, 432.
[2] F. H. Westheimer, *Science* **1987**, *235*, 1173.
[3] S. A. Strobel, J. C. Cochrane, *Curr. Opin. Chem. Biol.* **2007**, *11*, 636.
[4] T. Strassner, *Angew. Chem.* **2006**, *118*, 6570; *Angew. Chem. Int. Ed.* **2006**, *45*, 6420.
[5] A. Kohen, H.-H. Limbach, *Isotope Effects in Chemistry and Biology*, Taylor & Francis, Boca Raton, **2006**.
[6] A. C. Hengge, *Acc. Chem. Res.* **2002**, *35*, 105.
[7] K.-Y. Wong, J. P. Richard, J. Gao, *J. Am. Chem. Soc.* **2009**, *131*, 13963.
[8] Y. Liu, B. A. Gregersen, A. Hengge, D. M. York, *Biochemistry* **2006**, *45*, 10043.
[9] A. R. Ferré-D'Amaré, W. G. Scott, *Cold Spring Harbor Perspect. Biol.* **2010**, *2*, a003574.
[10] W. G. Scott, *Curr. Opin. Struct. Biol.* **2007**, *17*, 280.
[11] K.-Y. Wong, T.-S. Lee, D. M. York, *J. Chem. Theory Comput.* **2011**, *7*, 1.
[12] M. E. Harris, Q. Dai, H. Gu, D. L. Kellerman, J. A. Piccirilli, V. E. Anderson, *J. Am. Chem. Soc.* **2010**, *132*, 11613.

[13] S. Iyer, A. C. Hengge, *J. Org. Chem.* **2008**, *73*, 4819.
[14] H. M. Senn, W. Thiel, *Angew. Chem.* **2009**, *121*, 1220; *Angew. Chem. Int. Ed.* **2009**, *48*, 1198.
[15] W. F. van Gunsteren, D. Bakowies, R. Baron, I. Chandrasekhar, M. Christen, X. Daura, P. Gee, D. P. Geerke, A. Glättli, P. H. Hünenberger, M. A. Kastenholz, C. Oostenbrink, M. Schenk, D. Trzesniak, N. F. A. van der Vegt, H. B. Yu, *Angew. Chem.* **2006**, *118*, 4168; *Angew. Chem. Int. Ed.* **2006**, *45*, 4064.
[16] Z. Cao, Y. Mo, W. Thiel, *Angew. Chem.* **2007**, *119*, 6935; *Angew. Chem. Int. Ed.* **2007**, *46*, 6811.
[17] F. Claeyssens, J. N. Harvey, F. R. Manby, R. A. Mata, A. J. Mulholland, K. E. Ranaghan, M. Schutz, S. Thiel, W. Thiel, H.-J. Werner, *Angew. Chem.* **2006**, *118*, 7010; *Angew. Chem. Int. Ed.* **2006**, *45*, 6856.
[18] M. Cossi, G. Scalmani, N. Rega, V. Barone, *J. Chem. Phys.* **2002**, *117*, 43.
[19] J. W. Gaynor, R. Cosstick, *Curr. Org. Chem.* **2008**, *12*, 291.
[20] S. R. Das, J. A. Piccirilli, *Nat. Chem. Biol.* **2005**, *1*, 45.
[21] H. Kleinert, *Path Integrals in Quantum Mechanics, Statistics, Polymer Physics, and Financial Markets*, 3rd ed., World Scientific, Singapore, **2004**.
[22] K.-Y. Wong, J. Gao, *J. Chem. Phys.* **2007**, *127*, 211103.
[23] K.-Y. Wong, J. Gao, *J. Chem. Theory Comput.* **2008**, *4*, 1409.
[24] B. R. Brooks, C. L. Brooks III, A. D. Mackerell, Jr., L. Nilsson, R. J. Petrella, B. Roux, Y. Won, G. Archontis, C. Bartels, S. Boresch, A. Caflisch, L. Caves, Q. Cui, A. R. Dinner, M. Feig, S. Fischer, J. Gao, M. Hodoscek, W. Im, K. Kuczera, T. Lazaridis, J. Ma, V. Ovchinnikov, E. Paci, R. W. Pastor, C. B. Post, J. Z. Pu, M. Schaefer, B. Tidor, R. M. Venable, H. L. Woodcock, X. Wu, W. Yang, D. M. York, M. Karplus, *J. Comput. Chem.* **2009**, *30*, 1545.
[25] Y. Shao, L. F. Molnar, Y. Jung, J. Kussmann, C. Ochsenfeld, S. T. Brown, A. T. B. Gilbert, L. V. Slipchenko, S. V. Levchenko, D. P. O'Neill, R. A. DiStasio, Jr., R. C. Lochan, T. Wang, G. J. O. Beran, N. A. Besley, J. M. Herbert, C. Y. Lin, T. Van Voorhis, S. H. Chien, A. Sodt, R. P. Steele, V. A. Rassolov, P. E. Maslen, P. P. Korambath, R. D. Adamson, B. Austin, J. Baker, E. F. C. Byrd, H. Dachsel, R. J. Doerksen, A. Dreuw, B. D. Dunietz, A. D. Dutoi, T. R. Furlani, S. R. Gwaltney, A. Heyden, S. Hirata, C.-P. Hsu, G. Kedziora, R. Z. Khalliulin, P. Klunzinger, A. M. Lee, M. S. Lee, W. Liang, I. Lotan, N. Nair, B. Peters, E. I. Proynov, P. A. Pieniazek, Y. M. Rhee, J. Ritchie, E. Rosta, C. D. Sherrill, A. C. Simmonett, J. E. Subotnik, H. L. Woodcock III, W. Zhang, A. T. Bell, A. K. Chakraborty, D. M. Chipman, F. J. Keil, A. Warshel, W. J. Hehre, H. F. Schaefer III, J. Kong, A. I. Krylov, P. M. W. Gill, M. Head-Gordon, *Phys. Chem. Chem. Phys.* **2006**, *8*, 3172.
[26] D. A. McQuarrie, *Statistical Mechanics*, University Science Books, Sausalito, CA, USA **2000**.
[27] L. J. Schaad, L. Bytautas, K. N. Houk, *Can. J. Chem.* **1999**, *77*, 875.
[28] M. Wolfsberg in *Isotope Effects in Chemistry and Biology* (Eds.: A. Kohen, H.-H. Limbach), Taylor & Francis, Boca Raton, **2006**, p. 89.
[29] Y. Liu, B. A. Gregersen, X. Lopez, D. M. York, *J. Phys. Chem. B* **2005**, *109*, 19987.
[30] X. Liu, C. B. Reese, *Tetrahedron Lett.* **1996**, *37*, 925.
[31] X. Liu, C. B. Reese, *J. Chem. Soc. Perkin Trans. 1* **2000**, 2227.
[32] A. C. Hengge, I. Onyido, *Curr. Org. Chem.* **2005**, *9*, 61.
[33] M. A. Anderson, H. Shim, F. M. Raushel, W. W. Cleland, *J. Am. Chem. Soc.* **2001**, *123*, 9246.
[34] G. A. Sowa, A. C. Hengge, W. W. Cleland, *J. Am. Chem. Soc.* **1997**, *119*, 2319.
[35] C. S. López, O. N. Faza, A. R. de Lera, D. M. York, *Chem. Eur. J.* **2005**, *11*, 2081.
[36] X. Liu, C. B. Reese, *Tetrahedron Lett.* **1995**, *36*, 3413.
[37] J. B. Thomson, B. K. Patel, V. Jimenez, K. Eckart, F. Eckstein, *J. Org. Chem.* **1996**, *61*, 6273.

